JEM Journal of Experimental Medicine

BRIEF DEFINITIVE REPORT

Neutrophil-specific gain-of-function mutations in *Nlrp3* promote development of cryopyrin-associated periodic syndrome

Julien Stackowicz[1,2*], Nicolas Gaudenzio[3*], Nadine Serhan[3], Eva Conde[1], Ophélie Godon[1], Thomas Marichal[4], Philipp Starkl[5,6], Bianca Balbino[1,2], Axel Roers[7], Pierre Bruhns[1], Friederike Jönsson[1], Philippe Moguelet[8], Sophie Georgin-Lavialle[9], Lori Broderick[10], Hal M. Hoffman[10], Stephen J. Galli[11,12,13], and Laurent L. Reber[1,3]

Gain-of-function mutations in NLRP3 are responsible for a spectrum of autoinflammatory diseases collectively referred to as "cryopyrin-associated periodic syndromes" (CAPS). Treatment of CAPS patients with IL-1–targeted therapies is effective, confirming a central pathogenic role for IL-1β. However, the specific myeloid cell population(s) exhibiting inflammasome activity and sustained IL-1β production in CAPS remains elusive. Previous reports suggested an important role for mast cells (MCs) in this process. Here, we report that, in mice, gain-of-function mutations in *Nlrp3* restricted to neutrophils, and to a lesser extent macrophages/dendritic cells, but not MCs, are sufficient to trigger severe CAPS. Furthermore, in patients with clinically established CAPS, we show that skin-infiltrating neutrophils represent a substantial biological source of IL-1β. Together, our data indicate that neutrophils, rather than MCs, can represent the main cellular drivers of CAPS pathology.

Introduction

The NLRP3 inflammasome is a protein complex responsible for caspase-1–dependent release of IL-1β and IL-18 (Jo et al., 2016; Latz et al., 2013; Tschopp and Schroder, 2010). Gain-of-function mutations in NLRP3 are responsible for a spectrum of autoinflammatory diseases collectively referred to as "cryopyrin-associated periodic syndromes" (CAPS) or "*NLRP3*-associated autoinflammatory diseases" (Aksentijevich et al., 2002; Dowds et al., 2004; Hoffman et al., 2001a; Louvrier et al., 2020). These mutations in the NLRP3 gene cause constitutive activation of the NLRP3 inflammasome, leading to enhanced activation of caspase-1 and secretion of IL-1β and IL-18 (Agostini et al., 2004). Treatment of CAPS patients with IL-1–targeted therapies is effective (Fenini et al., 2017; Hoffman et al., 2004; Hoffman et al., 2012; Hoffman et al., 2008; Lachmann et al., 2009), confirming a central pathogenic role for IL-1β. Previous reports using mouse models of CAPS indicate that mutation of *Nlrp3* in myeloid cells is responsible for disease pathogenesis (Brydges et al., 2009; Meng et al., 2009). However, the specific myeloid cell population(s) exhibiting inflammasome activity and sustained IL-1β production in CAPS remains elusive.

CAPS encompasses a continuum of disease severity, characterized by fever, urticaria-like skin rashes, and systemic inflammation (Aksentijevich et al., 2007; Neven et al., 2004), and includes familial cold autoinflammatory syndrome (FCAS), Muckle-Wells syndrome (MWS), and neonatal-onset multisystem inflammatory disease (Neven et al., 2004). The urticaria-like skin rash observed in CAPS is similar to that associated with common urticaria, a disorder thought to depend largely on histamine released by mast cell (MC) activation. It has previously been reported that MC deficiency can reduce skin inflammation

[1]Unit of Antibodies in Therapy and Pathology, Institut Pasteur, UMR 1222, Institut national de la santé et de la recherche médicale, Paris, France; [2]Sorbonne Université, Paris, France; [3]Toulouse Institute for Infectious and Inflammatory Diseases (Infinity), Institut national de la santé et de la recherche médicale, UMR 1291, Centre National de la Recherche Scientifique, UMR 5051, University of Toulouse III, Toulouse, France; [4]GIGA-Research and Faculty of Veterinary Medicine, Liège University, Liège, Belgium; [5]Research Center for Molecular Medicine of the Austrian Academy of Sciences, Vienna, Austria; [6]Research Laboratory of Infection Biology, Department of Medicine I, Medical University of Vienna, Vienna, Austria; [7]Institute for Immunology, Medical Faculty Carl Gustav Carus, University of Technology Dresden, Dresden, Germany; [8]Faculty of Medicine, Sorbonne University, Tenon Hospital, Assistance Publique – Hôpitaux de Paris, Paris, France; [9]Internal Medicine Department, Tenon Hospital, Assistance Publique – Hôpitaux de Paris, Sorbonne University, Paris, France; [10]Division of Pediatric Allergy, Immunology and Rheumatology, University of California, San Diego, and Rady Children's Hospital, San Diego, CA; [11]Department of Pathology, Stanford University School of Medicine, Stanford, CA; [12]Department of Microbiology and Immunology, Stanford University School of Medicine, Stanford, CA; [13]Sean N. Parker Center for Allergy and Asthma Research, Stanford University School of Medicine, Stanford, CA.

*J. Stackowicz and N. Gaudenzio contributed equally to this work; Correspondence to Laurent L. Reber: laurent.reber@inserm.fr; Stephen J. Galli: sgalli@stanford.edu; Hal M. Hoffman: hahoffman@health.ucsd.edu.

in mice expressing the *Nlrp3*^{R258W} mutation, corresponding to the R260W mutation found in some MWS patients (Nakamura et al., 2012). In this model of CAPS, *Nlrp3* mutant mice developed skin inflammation over several weeks (Meng et al., 2009). Additional CAPS mouse models have been reported, with different mutations in *Nlrp3* inducing more severe pathology, characterized by the development of skin inflammation within a few days after birth, poor growth, and perinatal mortality (Brydges et al., 2009). However, because human CAPS represents a spectrum of diseases of different severity, the relative contributions of MCs might potentially depend on the nature of the *Nlrp3* mutation and/or on the severity of the pathology.

Both monocytes/macrophages and dendritic cells (DCs) have been used extensively to study the mechanism of activation of the NLRP3 inflammasome (Kool et al., 2008; Martinon et al., 2002; Martinon et al., 2006; Sharp et al., 2009). In addition, macrophages from CAPS patients were shown to spontaneously secrete IL-1β (Agostini et al., 2004; Camilli et al., 2020). However, whether macrophages and/or DCs play a key role in CAPS remains to be fully determined.

Blood neutrophilia and neutrophil infiltration in several tissues are hallmarks of CAPS (Hoffman and Broderick, 2016; Hoffman et al., 2001b; Ley et al., 2018). It was reported that levels of neutrophil secretory proteins are significantly elevated in the plasma of mice harboring a CAPS-associated *Nlrp3*^{A350V} mutation (Johnson et al., 2017). However, the functions of neutrophils in CAPS remain largely unknown. Here we report that, in mice, *Nlrp3*^{A350V} and *Nlrp3*^{L351P} mutations, which mirror two clinically established mutations associated with MWS (A352V) and FCAS (L353P), respectively (Brydges et al., 2009), restricted to neutrophils but not MCs, are sufficient to trigger severe CAPS. Furthermore, in patients with clinically established CAPS, we show that skin-infiltrating neutrophils represent a substantial biological source of IL-1β. Together, our data indicate that neutrophils, rather than MCs, can represent the main cellular drivers of CAPS pathology.

Results and discussion

MCs are not required for the development of CAPS driven by Nlrp3 A350V or L351P mutations in mice

Mutations of *Nlrp3* in myeloid cells are responsible for CAPS pathogenesis in mice (Brydges et al., 2009; Meng et al., 2009). To achieve expression of NLRP3 mutant proteins in myeloid cells, we crossed *Nlrp3*^{A350V}*NeoR*$^{fl/fl}$ mice with transgenic mice expressing Cre recombinase under the control of the lysozyme 2 promoter (*Lys*). To test whether MCs played a role in this myeloid cell–induced CAPS model, we crossed *Nlrp3*^{A350V} *Lys-Cre* mice with *Kit*$^{W\text{-}sh/W\text{-}sh}$ MC-deficient mice to generate triple-transgenic littermate mice expressing the *Nlrp3*^{A350V} mutation under the control of the *Lys* promoter in either MC-deficient (*Kit*$^{W\text{-}sh/W\text{-}sh}$) or MC-sufficient backgrounds (*Kit*$^{W\text{-}sh/+}$). As reported previously, *Nlrp3*^{A350V} *Lys-Cre* mice had severe growth delay and died within 2 wk of birth (Brydges et al., 2009; Fig. 1, A–C). As expected, MC numbers were markedly reduced in the skin of *Kit*$^{W\text{-}sh/W\text{-}sh}$ *Nlrp3*^{A350V} *Lys-Cre* mice as compared with *Kit*$^{W\text{-}sh/+}$ *Nlrp3*^{A350V} *Lys-Cre* mice (Fig. 1 A). However, no noticeable differences in skin pathology, body weight, or survival were observed in *Nlrp3*^{A350V} mutant MC-sufficient versus MC-deficient mice, and all mice died within 2 wk after birth (Fig. 1, A–C). *Nlrp3*^{A350V} *Lys-Cre*$^{+}$ mice had slightly increased numbers of MCs in the skin as compared with Cre-negative controls (Fig. S1, A and B). However, <20% of these MCs in the skin of *Nlrp3*^{A350V} *Lys-Cre*$^{+}$ mice expressed IL-1β (Fig. S1, A and C).

We used the same approach with the FCAS-associated *Nlrp3*^{L351P}*NeoR*$^{fl/fl}$ mutant mouse model. When crossed to *Lys-Cre* mice, the resulting mutants displayed a more severe phenotype, because very few mice survived within 1 or 2 d of birth (Brydges et al., 2009). We observed the same phenotype in the MC-deficient *Kit*$^{W\text{-}sh/W\text{-}sh}$ *Nlrp3*^{L351P} *Lys-Cre* mice: Among the 25 mice born, only 3 survived until day 1, and all died by day 2 (Fig. 1 D). Altogether, our data suggest that MCs are not required for the development of pathology induced by myeloid cells in these two severe CAPS models.

Previous reports indicate that mouse MCs expressing CAPS-associated *Nlrp3* mutations can produce IL-1β (Nakamura et al., 2012; Nakamura et al., 2009). However, *Lys-Cre* mice do not express the Cre recombinase in MCs (Abram et al., 2014). Thus, to study further the in vivo effects of a CAPS-associated *Nlrp3* mutation in MCs, we generated a mouse model in which the pathogenic *Nlrp3* mutation was restricted to MCs (i.e., by crossing *Nlrp3*^{L351P}*NeoR*$^{fl/fl}$ mice with *Mcpt5-Cre* mice, which express Cre recombinase under the control of the connective tissue MC-specific MC protease 5 [*Mcpt5*] promoter; Dudeck et al., 2011). Interestingly, *Nlrp3*^{L351P} *Mcpt5-Cre* mice did not develop any observable signs of skin inflammation and survived normally (mice were monitored for up to 1 yr after birth; Fig. 1, E and F). This supports the conclusion that a MC-restricted *Nlrp3* L351P mutation is not sufficient to drive CAPS in mice. In addition, *Nlrp3*^{L351P} *Mcpt5-Cre*$^{+}$ and *Nlrp3*^{L351P} *Mcpt5-Cre*$^{-}$ mice had similar numbers of skin MCs (Fig. 1 E) and similar responses in a model of IgE-mediated passive systemic anaphylaxis (PSA; Fig. S1 D) that largely depends on MCs (Finkelman, 2007; Reber et al., 2017b). This indicates that, under the conditions tested, the *Nlrp3*^{L351P} mutation in MCs had no significant effect on IgE-mediated effector functions.

Our results differ significantly from those of Nakamura et al., who demonstrated that MCs harboring an R258W gain-of-function *Nlrp3* mutation importantly contributed to CAPS pathogenesis in mice (Nakamura et al., 2012). Several factors might account for such differences. For example, the A350V or L351P *Nlrp3* mutations that we studied confer a more severe phenotype than the R258W mutation in mice (Brydges et al., 2009; Nakamura et al., 2012). Indeed, we and others reported that, in several disease models, MCs can amplify inflammation in models of moderate severity, whereas other cells may mask any contributions of MCs in more severe models (Reber et al., 2012). In addition, Nakamura et al. reported that the microbiome can play an important role in the development of CAPS in *Nlrp3*^{R258W} mice (Nakamura et al., 2012). Therefore, it is possible that differences in the microbiota might account, at least in part, for the different results obtained.

We also derived MCs in vitro from circulating CD34^{+} hematopoietic progenitors from the blood of different CAPS patients

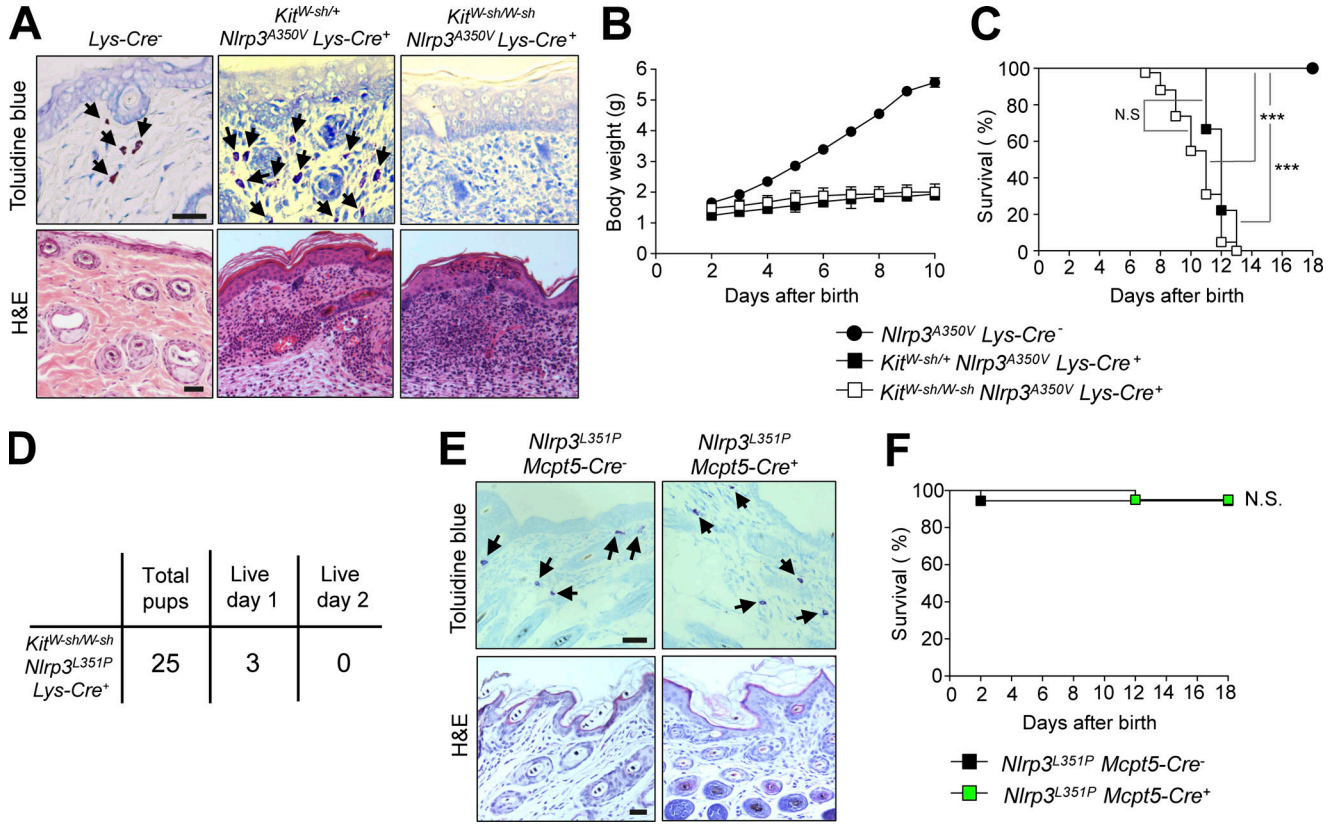

Figure 1. **MCs are not required for the development of severe CAPS in mice.** *Nlrp3*^{A350V} *Lys-Cre* mice were crossed with MC-deficient *Kit*$^{W\text{-}sh/W\text{-}sh}$ mice to generate littermate mice expressing the *Nlrp3*^{A350V} mutation in an MC-sufficient (*Kit*$^{W\text{-}sh/+}$) or an MC-deficient (*Kit*$^{W\text{-}sh/W\text{-}sh}$) background. **(A)** Toluidine blue staining (assessing MCs) and H&E staining (assessing leukocyte infiltration) of skin sections from *Kit*$^{W\text{-}sh/+}$ *Nlrp3*^{A350V} *Lys-Cre*$^{+}$ and *Kit*$^{W\text{-}sh/W\text{-}sh}$ *Nlrp3*^{A350V} *Lys-Cre*$^{+}$ or *Lys-Cre*$^{-}$ control mice. Black arrows indicate MCs. **(B)** Body weight at the indicated time points after birth in *Nlrp3*^{A350V} *Lys-Cre*$^{-}$ control mice (data are pooled from *Kit*$^{W\text{-}sh/W\text{-}sh}$ and *Kit*$^{W\text{-}sh/+}$ backgrounds; n = 40 at day 0), MC-sufficient *Kit*$^{W\text{-}sh/+}$ *Nlrp3*^{A350V} *Lys-Cre*$^{+}$ mice (n = 6 at day 0), and MC-deficient *Kit*$^{W\text{-}sh/W\text{-}sh}$ *Nlrp3*^{A350V} *Lys-Cre*$^{+}$ mice (n = 7 at day 0). Data are presented as mean ± SEM. **(C)** Survival of *Nlrp3*^{A350V} *Lys-Cre*$^{-}$ control mice (n = 29), *Kit*$^{W\text{-}sh/+}$ *Nlrp3*^{A350V} *Lys-Cre*$^{+}$ mice (n = 9), and MC-deficient *Kit*$^{W\text{-}sh/W\text{-}sh}$ *Nlrp3*^{A350V} *Lys-Cre*$^{+}$ mice (n = 42). ***, P < 0.001 using the Mantel-Haenszel log-rank test. **(D)** Birth table of *Kit*$^{W\text{-}sh/W\text{-}sh}$ *Nlrp3*^{L351P} *Lys-Cre*$^{+}$ pups. Shown are total live pups at birth and total pups on days 1 and 2 after birth. **(E)** Toluidine blue staining (assessing MCs) and H&E staining (assessing leukocyte infiltration) of skin sections from 8-wk-old *Nlrp3*^{L351P} *Mcpt5-Cre*$^{-}$ (n = 18) and *Nlrp3*^{L351P} *Mcpt5-Cre*$^{+}$ (n = 21) mice. Black arrows indicate MCs. **(F)** Survival of *Nlrp3*^{L351P} *Mcpt5-Cre*$^{-}$ and *Nlrp3*^{L351P} *Mcpt5-Cre*$^{+}$ mice. N.S., P > 0.05. Scale bars: 50 µm.

and healthy donors (Fig. S1 E). Although we observed a slight increase in IgE-mediated degranulation dynamics of MCs from CAPS patients compared with healthy donors (Fig. S1, F and G), none of these MCs released detectable amounts of IL-1β upon classical stimulation of the NLRP3 pathway with LPS (Fig. S1 H). Altogether, these data suggest that MCs do not represent an important source of IL-1β in CAPS.

Expression of Nlrp3 and Il1b genes among immune cells

To identify which cell type(s) exhibited mRNA associated with increased inflammasome activity and IL-1β production in mice, we mapped the expression of *Nlrp3* and *Il1b* genes among various subpopulations of mouse immune cells, using publicly available RNA-sequencing data (Heng et al., 2008). This analysis showed that neutrophils, DCs, monocytes, and basophils, but not MCs, represent potential major sources of NLRP3 in mice and that neutrophils are likely to represent the main source of IL-1β among the 21 purified mouse immune cell populations analyzed (Fig. S2 A). In line with these findings, we also found that human granulocytes, DCs, and monocytes express high levels of *NLRP3* and *IL1B* mRNA in similar RNA microarray data (Shay et al., 2013; Fig. S2 B).

Contribution of DCs and macrophages to IL-1β production and CAPS pathogenesis

Nlrp3^{A350V} *Lys-Cre*$^{+}$ mice had a marked increase in numbers of skin macrophages compared with Cre^{-} controls (Fig. 2, A and B). However, <10% of these macrophages were positive for IL-1β (Fig. 2 C). By contrast, between 20% and 40% of skin CD11c^{+} DCs stained positive for IL-1β (Fig. 2, D–F).

On the basis of these findings, we decided to use *Cd11c-Cre* mice to assess the potential contributions of DCs and macrophages. Cd11c-Cre mice were reported to express Cre in DCs (85–90% of conventional DCs and plasmacytoid DCs in the spleen) and also in macrophages (>95% alveolar macrophages and ∼70% red pulp macrophages), but not in MCs, neutrophils, or other granulocytes (Abram et al., 2014). In marked contrast with our data in *Lys-Cre* mice, we found that *Cd11c-Cre*$^{+}$*; Nlrp3*^{A350V} pups gained weight and survived normally, indicating that restricting the A350V mutation to macrophages and DCs is

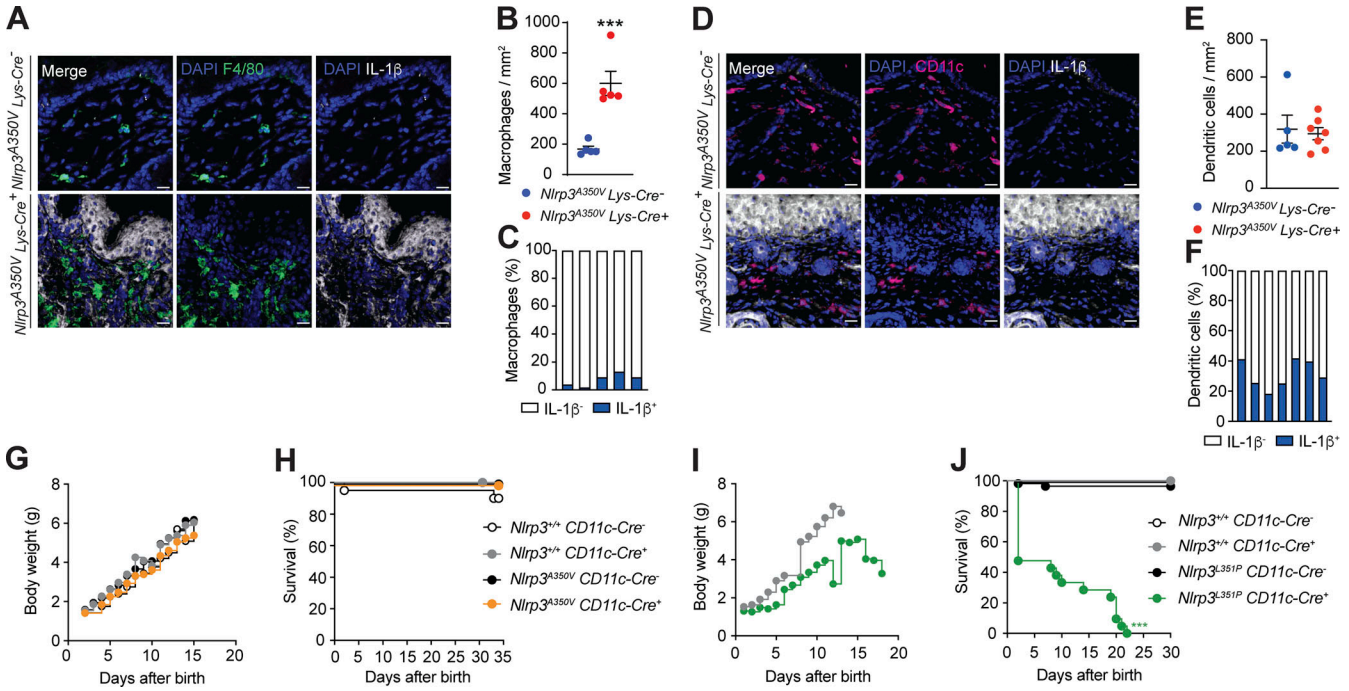

Figure 2. **Evidence that DCs participate in CAPS-like syndrome induced by the *Nlrp3* L351P but not the *Nlrp3* A350V mutation in mice. (A)** Representative confocal microscopy showing staining of skin tissue sections from *Nlrp3*^{A350V} *Lys-Cre*$^{+}$ mice and *Nlrp3*^{A350V} *Lys-Cre*$^{-}$ controls stained with DAPI (which stains nuclei), anti–IL-1β antibodies, and anti-F4/80 antibodies (which stain macrophages). Scale bars, 20 µm. **(B)** Quantification of F4/80^{+} macrophages in skin sections. Data represent values from individual mice, with bars indicating mean ± SEM. ***, P < 0.001 (Mann-Whitney *U* test). **(C)** Percentage of IL-1β^{+} and IL-1β^{-} macrophages (F4/80^{+}) in skin sections. **(D)** Representative confocal microscopy showing staining of skin tissue sections from *Nlrp3*^{A350V} *Lys-Cre*$^{+}$ mice and *Nlrp3*^{A350V} *Lys-Cre*$^{-}$ controls stained with DAPI (which stains nuclei), anti–IL-1β antibodies, and anti-CD11c antibodies (which stain DCs). Scale bars, 20 µm. **(E)** Quantification of CD11c^{+} DCs in skin sections. Data represent values from individual mice with bars indicating mean ± SEM. **(F)** Percentage of IL-1β^{+} and IL-1β^{-} DCs (CD11c^{+}) in skin sections. **(G)** Body weight at the indicated time points after birth in *Nlrp3*$^{+/+}$ *Cd11c-Cre*$^{-}$ (n = 12 at day 0), *Nlrp3*$^{+/+}$ *Cd11c-Cre*$^{+}$ (n = 6 at day 0), *Nlrp3*^{A350V} *Cd11c-Cre*$^{-}$ (n = 10 at day 0), and *Nlrp3*^{A350V} *Cd11c-Cre*$^{+}$ mice (n = 10 at day 0). **(H)** Survival of *Nlrp3*$^{+/+}$ *Cd11c-Cre*$^{-}$ (n = 20 at day 0), *Nlrp3*$^{+/+}$ *Cd11c-Cre*$^{+}$ (n = 19 at day 0), *Nlrp3*^{A350V} *Cd11c-Cre*$^{-}$ (n = 19 at day 0), and *Nlrp3*^{A350V} *Cd11c-Cre*$^{+}$ mice (n = 17 at day 0). **(I)** Body weight at the indicated time points after birth in *Nlrp3*^{WT} *Cd11c-Cre*$^{-}$ (n = 3 at day 0), *Nlrp3*$^{+/+}$ *Cd11c-Cre*$^{+}$ (n = 7 at day 0), *Nlrp3*^{L351P} *Cd11c-Cre*$^{-}$ (n = 9 at day 0), and *Nlrp3*^{L351P} *Cd11c-Cre*$^{+}$ mice (n = 6 at day 0). **(J)** Survival of *Nlrp3*$^{+/+}$ *Cd11c-Cre*$^{-}$ (n = 7 at day 0), *Nlrp3*$^{+/+}$ *Cd11c-Cre*$^{+}$ (n = 9 at day 0), *Nlrp3*^{L351P} *Cd11c-Cre*$^{-}$ (n = 57 at day 0), and *Nlrp3*^{L351P} *Cd11c-Cre*$^{+}$ mice (n = 21 at day 0).

not sufficient to induce a CAPS-like phenotype in mice (Fig. 2, G and H). We also generated *Cd11c-Cre*$^{+}$*; Nlrp3*^{L351P} mice. Interestingly, these mice did develop a CAPS-like phenotype, with reduced body weight and perinatal mortality (Fig. 2, I and J). However, the phenotype was less severe than that observed in *Lys-Cre* mice, because all *Lys-Cre*$^{+}$*; Nlrp3*^{L351P} mice died within 2 d after birth (Brydges et al., 2009; Fig. 1 D), whereas some *Cd11c-Cre*$^{+}$*; Nlrp3*^{L351P} mice survived for up to 22 d (Fig. 2 J).

Evidence that neutrophils represent an important source of IL-1β in CAPS

A previous report indicated that neutrophil secretory proteins, including myeloperoxidase (MPO), are significantly elevated in the plasma of mice with a tamoxifen-inducible *Nlrp3*^{A350V} mutation (Johnson et al., 2017). This observation suggested that the pathology in this model might be associated with neutrophil activation. In line with these results, we observed elevated numbers of neutrophils in the blood and skin of *Nlrp3*^{A350V} *Lys-Cre*$^{+}$ mice (Fig. 3, A–C). Importantly, a large proportion of the skin neutrophils were strongly positive for IL-1β (Fig. 3 D). These results indicate that neutrophils, rather than MCs, represent an important source of IL-1β in this severe CAPS model. Because the antibody we used recognizes both pro–IL-1β and active IL-1β, we also stained skin samples with an antibody recognizing pro–caspase-1 and active caspase-1 (upon cleavage at Asp210). Almost all caspase-1^{+} cells were neutrophils, confirming that neutrophils might be a major source of inflammasome activity in *Nlrp3*^{A350V} *Lys-Cre*$^{+}$ mice (Fig. S2, C and D). Activation of the NLRP3 inflammasome also leads to IL-18 release, and IL-18 contributes to the CAPS-like phenotype in both *Nlrp3*^{A350V} *Lys-Cre* and *Nlrp3*^{L351P} *Lys-Cre* mice (Brydges et al., 2013). We found that ∼45% of neutrophils stained positive for IL-18 in the skin of *Nlrp3*^{A350V} *Lys-Cre* mice. However, >90% of all other cells were also IL-18^{+}, indicating that this cytokine is potentially produced by many cell populations in *Nlrp3*^{A350V} *Lys-Cre* mice (Fig. S2, E and F).

In accord with these results, neutrophils freshly purified from the peripheral blood of CAPS patients released IL-1β at levels slightly (but not significantly) higher than neutrophils from healthy donors (Fig. S2, G and H). By contrast, none of these cells released detectable amounts of IL-18 (Fig. S2 I). We also observed substantial infiltration of neutrophils in skin biopsies from CAPS patients (Fig. 3, E and F; and Fig. S2 J), and ∼60% of these neutrophils were strongly positive for IL-1β (Fig. 3, E and G; and Fig. S2 J). Altogether, our data suggest that neutrophils are major IL-1β producers in CAPS and thus might play a key role in CAPS pathology.

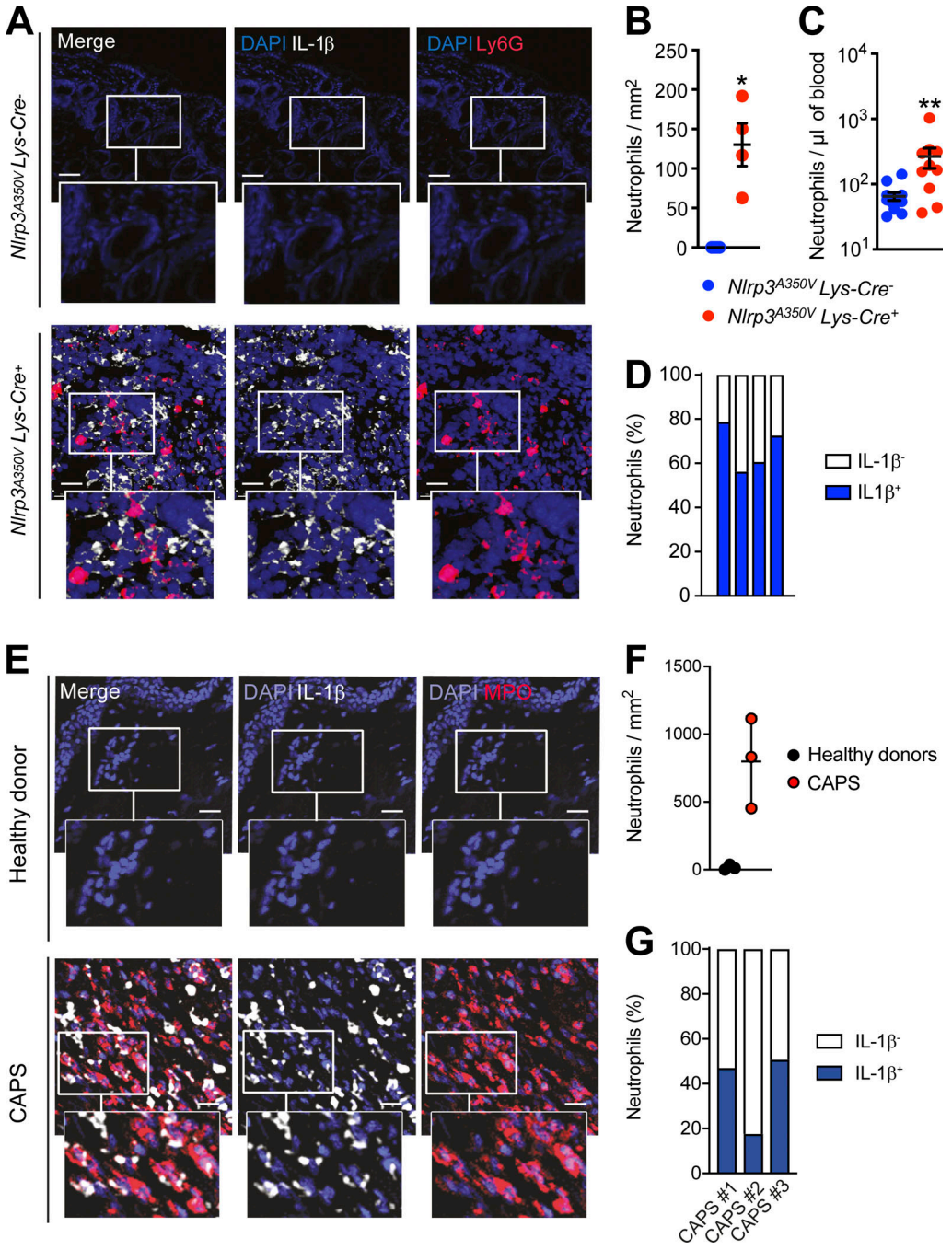

Figure 3. **Neutrophils are an important source of IL-1β in the skin of *Nlrp3*^{A350V} *Lys-Cre* mice and CAPS patients. (A)** Representative confocal microscopy showing staining of skin tissue sections from *Nlrp3*^{A350V} *Lys-Cre*$^{+}$ mice and *Nlrp3*^{A350V} *Lys-Cre*$^{-}$ controls stained with DAPI (which stains nuclei), anti–IL-1β antibodies, and anti-Ly6G antibodies (which stain neutrophils). Lower panels are enlargements of the boxed areas. Scale bars, 100 µm. **(B)** Quantification of Ly6G^{+} neutrophils in skin sections. **(C)** Quantification of Ly6G^{+}CD11b^{+} neutrophils in the blood from 7-d-old *Nlrp3*^{A350V} *Lys-Cre*$^{+}$ and *Nlrp3*^{A350V} *Lys-Cre*$^{-}$ mice (n = 10/group). Results in B and C show values from individual mice, with bars indicating mean ± SEM. *, P < 0.05; **, P < 0.01 (Mann-Whitney *U* test). **(D)** Percentage of IL-1β^{+} and IL-1β^{-} neutrophils (Ly6G^{+}) in skin sections. **(E)** Confocal microscopy showing staining of skin tissue sections from one healthy donor and one CAPS patient stained with DAPI (to indicate nuclei), anti–IL-1β antibodies, and anti-MPO, which is mainly produced by neutrophils. Scale bars, 50 µm. Lower panels are enlargements of the boxed areas. **(F)** Quantification of MPO^{+} neutrophils in the skin from CAPS patients and healthy donors. **(G)** Percentage of IL-1β^{+} and IL-1β^{-} neutrophils (MPO^{+}) in skin sections from three CAPS patients. Representative skin sections from CAPS patients 2 and 3 are depicted in Fig. S3 E.

Neutrophil-intrinsic Nlrp3 mutation triggers development of CAPS

To further investigate the role of neutrophils in CAPS, we crossed *Nlrp3*^{A350V} *NeoR*$^{fl/+}$ mice with neutrophil-specific *MRP8-Cre* mice (Passegué et al., 2004; Reber et al., 2017a), generating mice with a gain-of-function mutation in *Nlrp3* restricted to neutrophils. Indeed, previous reports indicate that *MRP8-Cre* mice express at baseline Cre recombinase in ∼90% of blood neutrophils and ∼80% of neutrophils in the spleen and bone marrow (Abram et al., 2014; Reber et al., 2017a). *Nlrp3*^{A350V}

MRP8-Cre mice exhibited a severe skin inflammatory phenotype and substantial reduction in body weight, exhibited blood neutrophilia, and died within 2 wk of birth (Fig. 4, A–D). This phenotype was very similar to that observed in myeloid-restricted *Nlrp3*^{A350V} *Lys-Cre* mice (Fig. 1, A–C).

MRP8-Cre mice have an internal ribosome entry site–GFP reporter that can be used to track Cre-expressing cells (Passegué et al., 2004; Reber et al., 2017a). We confirmed that GFP expression was restricted to Ly6G$^+$ neutrophils in the blood of *Nlrp3*^{A350V} *MRP8-Cre* mice (Fig. 4 E). *Nlrp3*^{A350V} *MRP8-Cre* mice also had a strong infiltration of neutrophils in the skin (Fig. 4, F and G). In line with our previous observations in *Lys-Cre* mice (Fig. 3), most skin neutrophils stained positively for IL-1β (Fig. 4, F and H) and caspase-1 (Fig. S3, A and B).

To assess the respective contributions of IL-1β versus IL-18 to the CAPS-like phenotype observed in *Nlrp3*^{A350V} *MRP8-Cre* mice, we treated these mice, from days 2–12 after birth, every 2 d with neutralizing antibodies against IL-1β or IL-18 (Fig. S3 C). Treatment with anti–IL-18 antibodies had no detectable effect, because all mice gained no more than ∼2 g of body weight and died within 12 d (Fig. S3, D and E), a phenotype very similar to that observed in untreated *Nlrp3*^{A350V} *MRP8-Cre* mice (Fig. 1, B and C). Mice treated with the anti–IL-1β antibody gained slightly more weight, and 50% of the mice were still alive at day 14 (Fig. S3, D and E). However, all of these mice developed a clear CAPS-like phenotype. This suggests that, in mice with the *Nlrp3* A350V mutation restricted to neutrophils, either anti–IL-1β antibody did not fully block IL-1β in newborns or additional mediators also significantly contributed to the disease. Among these potential mediators, TNF was reported to contribute importantly to the CAPS-like phenotype in *Nlrp3*^{A350V} *Lys-Cre* mice (McGeough et al., 2017). Besides activation of IL-1β and IL-18, caspase-1 also cleaves and activates gasdermin D, a pore-forming protein that induces pyroptosis (Chen et al., 2018; Sollberger et al., 2018). Gasdermin D–induced pyroptosis thus may also contribute to the CAPS-like phenotype in *Nlrp3* mutant mice. In addition, the skin phenotype in *Nlrp3*^{A350V} *MRP8-Cre* mice is already evident at birth. Therefore, it is possible that starting anti–IL-1β or anti–IL-18 therapy at day 2 might be too late to permit full rescue of the phenotype in this model.

Finally, severe CAPS also developed in *Nlrp3*^{L351P} *MRP8-Cre* mice, with a strong infiltration of leukocytes, and increased numbers of MCs, in the skin (Fig. 4, I and J). However, although all *Nlrp3*^{L351P} *Lys-Cre* mice died within 2 d after birth (Brydges et al., 2009; Fig. 1 D), some *Nlrp3*^{L351P} *MRP8-Cre* mice survived for up to 1 wk after birth (Fig. 4 K). These results demonstrate that the neutrophil-intrinsic *Nlrp3* mutation is sufficient to trigger the development of the pathological features associated with these models of CAPS, but they also confirm that the *Nlrp3* mutation within additional myeloid cell population(s) such as macrophages and DCs (as revealed using *Cd11c-Cre* mice in Fig. 2, G and H) may contribute to the more severe phenotype associated with the *Nlrp3*^{L351P} mutation.

It remains to be fully determined why gain-of-function mutations in *Nlrp3* in neutrophils, and to a lesser extent in DCs or macrophages, but not in MCs, are sufficient to drive CAPS pathology. One potential explanation is that MCs lack expression of one or more genes required for optimal activation of the NLRP3 inflammasome. Furthermore, although neutrophils are virtually absent from healthy skin, these cells are the first leukocytes to be attracted at sites of inflammation and clearly represent the main immune cell population in the inflamed skin of CAPS patients and in our mouse models. This might explain why neutrophils represent the main driver of CAPS pathology, although DCs, macrophages, and likely additional cell populations can release IL-1β and display NLRP3 inflammasome activity.

Altogether, our data suggest that neutrophils may represent a novel therapeutic target in CAPS. Although fully depleting neutrophils would likely expose CAPS patients to unacceptably high risks of infection, blocking neutrophil recruitment could represent an efficient strategy to reduce skin inflammation in CAPS. CXCR2 is considered to be the dominant neutrophil chemokine receptor in humans, and several CXCR2 antagonists have already been tested in clinical trials (Németh et al., 2020). Although future studies are needed, these new therapeutics may represent a promising treatment for neutrophilic skin disease and may have beneficial effects in CAPS.

Materials and methods

Mice

MRP8-Cre/iresGFP mice (B6.Cg-*Tg(S100A8-cre,-EGFP)1Ilw/J*; Passegué et al., 2004; Reber et al., 2017a) were obtained from Irving Weissman (Stanford University, Stanford, CA) and Clifford Lowell (University of California, San Francisco, San Francisco, CA). *Kit*$^{W\text{-}sh/W\text{-}sh}$ mice (B6.Cg-*Kit*$^{W\text{-}sh}$/HNihrJaeBsmGlliJ), *Lys-Cre* mice (B6.129P2-*Lyz2*$^{tm1(cre)Ifo}$/J), and *Cd11c-Cre* mice (B6.Cg-Tg(*Itgax-cre*)1-1Reiz/J) were obtained from The Jackson Laboratory. *C57BL/6-Mcpt5-Cre*$^+$ mice (Dudeck et al., 2011) were provided by A. Roers. *NLRP3*^{A350VneoR} (B6.129-*Nlrp3*^{tm1Hhf}/J) and *Nlrp3*^{L351PneoR} mice (B6N.129-*Nlrp3*^{tm2Hhf}/J) have been described previously (Brydges et al., 2009). Mice were bred in the Institut Pasteur; University of California, San Diego; or Stanford University specific pathogen–free animal facilities. All animal care and experimentation were conducted in compliance with the guidelines of the National Institutes of Health and with the specific approval of the institutional animal care and use committees of Stanford University and the University of California, San Diego, and/or of the Committee for Ethics in Animal Experimentation (Institut Pasteur, Paris, France) registered under #C2EA-89.

Survival and growth assessment

Pup survival was calculated as the percentage of pups surviving from birth. Growth gain was determined by weighing the mice every day from birth.

Flow cytometry

We used flow cytometry to identify and enumerate neutrophils in the peripheral blood. RBCs were lysed by treatment with RBC lysis buffer (BD Biosciences). Neutrophils were stained on ice for 30 min with anti–Ly6G-BV412 (clone 1A8, 1:200; BioLegend) and anti–CD11b-APC Vio770 (clone M1/70.15.11.5, 1:50; Miltenyi Biotec) antibodies. In some experiments, we used the FITC channel for analysis of GFP expression. Dead cells (stained with

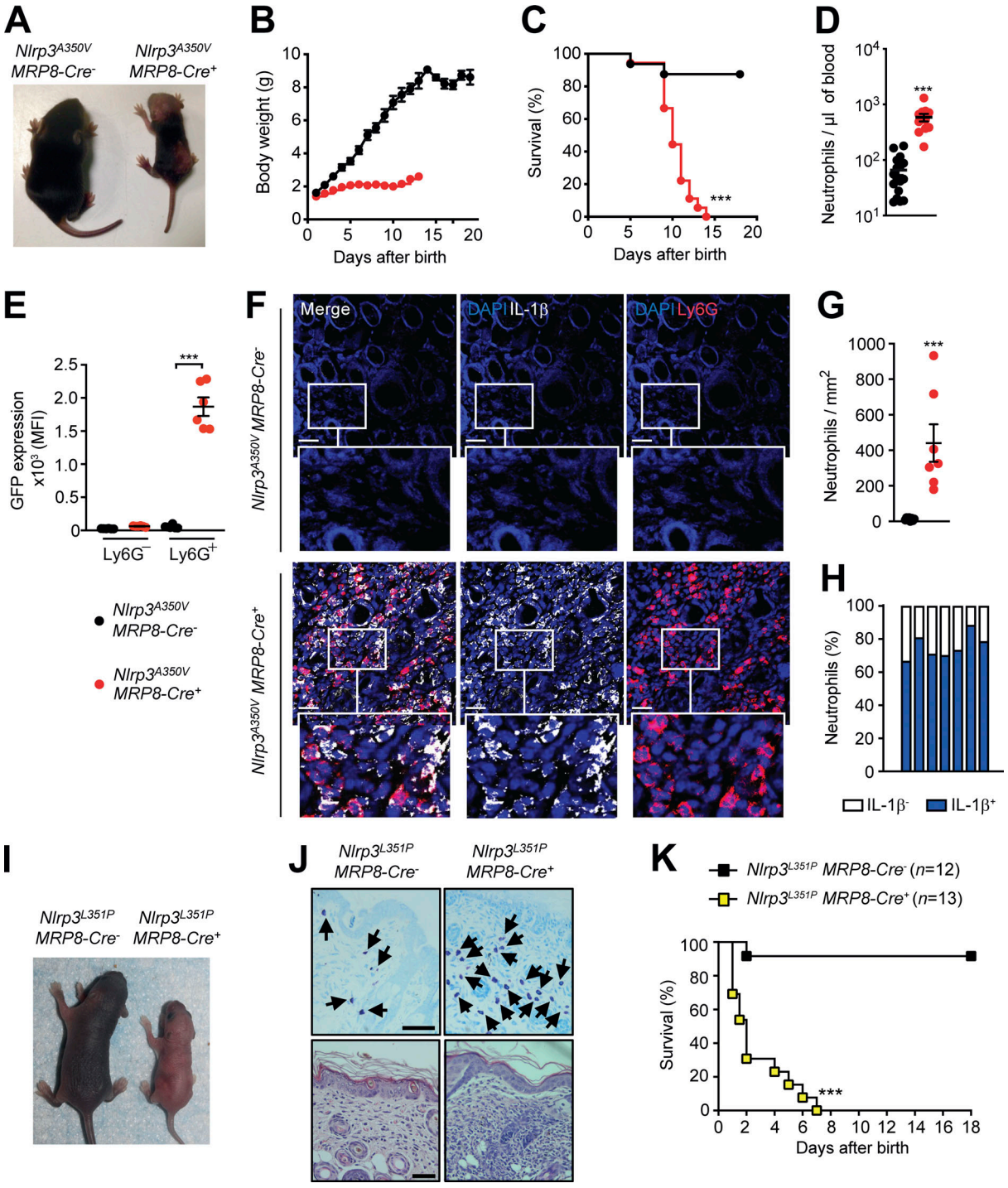

Figure 4. **Neutrophil-restricted gain-of-function mutation in *Nlrp3* promotes development of severe CAPS in mice. (A)** Representative picture of 7-d-old *Nlrp3*^{A350V} *MRP8-Cre*$^{-}$ and *Nlrp3*^{A350V} *MRP8-Cre*$^{+}$ mice. **(B)** Body weight at the indicated time points after birth in *Nlrp3*^{A350V} *MRP8-Cre*$^{-}$ (n = 11 at day 0) and *Nlrp3*^{A350V} *MRP8-Cre*$^{+}$ mice (n = 17 at day 0). **(C)** Survival of *Nlrp3*^{A350V} *MRP8-Cre*$^{-}$ (n = 16) and *Nlrp3*^{A350V} *MRP8-Cre*$^{+}$ mice (n = 18). **(D)** Quantification of Ly6G^{+} CD11b^{+} neutrophils in the blood of 7-d-old *Nlrp3*^{A350V} *MRP8-Cre*$^{+}$ mice (n = 11) and *Nlrp3*^{A350V} *MRP8-Cre*$^{-}$ controls (n = 17). Results show values from individual mice, with bars indicating mean ± SEM. **(E)** GFP expression (mean fluorescence intensity [MFI]) among Ly6G^{-} and Ly6G^{+} blood leukocytes in *Nlrp3*^{A350V} *MRP8-Cre*$^{+}$ mice and *Nlrp3*^{A350V} *MRP8-Cre*$^{-}$ controls (n = 6/group). **(F)** Representative confocal microscopy showing staining of skin sections from *Nlrp3*^{A350V} *MRP8-Cre*$^{+}$ mice and *Nlrp3*^{A350V} *MRP8-Cre*$^{-}$ controls stained with DAPI (which stains nuclei), anti–IL-1β antibodies, and anti-Ly6G antibodies (which stain neutrophils). Lower panels are enlargements of the boxed areas. Scale bars: 50 µm. **(G)** Quantification of Ly6G^{+} neutrophils in skin sections. Results show values from individual mice, with bars indicating mean ± SEM. **(H)** Percentage of IL-1β^{+} and IL-1β^{-} neutrophils (Ly6G^{+}) in skin sections. **(I)** Representative picture of 4-d-old *Nlrp3*^{L351P} *MRP8-Cre*$^{-}$ and *Nlrp3*^{L351P} *MRP8-Cre*$^{+}$ mice. **(J)** Representative toluidine blue staining (assessing MCs) and H&E staining (assessing leukocyte infiltration) of skin sections from 7-d-old *Nlrp3*^{L351P} *MRP8-Cre*$^{-}$ and *Nlrp3*^{L351P} *MRP8-Cre*$^{+}$ mice. Black arrows indicate MCs. **(K)** Survival of *Nlrp3*^{L351P} *MRP8-Cre*$^{-}$ (n = 12) and *Nlrp3*^{L351P} *MRP8-Cre*$^{+}$ mice (n = 13). ***, P < 0.001 using the Mantel-Haenszel log-rank test (in C and K) or Mann-Whitney U test (in D, E, and G). Scale bars: 100 µm.

Table 1. **Clinical characteristics of patients with CAPS**

Syndrome	Sex	Mutation	Age (yr)	Treatment	Figure
MWS	M	T436A	32	Canakinumab	Fig. S1, E–H
FCAS	F	L353P	86	Rilonacept	Fig. S1, E–H
FCAS	F	L353P	32	Rilonacept	Fig. S1, E–H
NOMID	M	G326E	13	Anakinra	Fig. S2, G–I
MWS	F	R260W	42	Canakinumab	Fig. S2, G–I
FCAS	F	L353P	74	Canakinumab	Fig. S2, G–I
FCAS?	F	V198M	46	–	Fig. S2 J
FCAS	M	A439V	48	Canakinumab	Fig. 3 E
MWS	F	Q567K	70	–	Fig. S2 J

F, female; M, male; NOMID, neonatal-onset multisystem inflammatory disease.

propidium iodide, 1:1,000) were not included in the analysis. Data were acquired using a MACSQuant flow cytometer (Miltenyi Biotec) and analyzed with FlowJo software (BD Biosciences).

Human samples

Skin biopsies from symptomatic CAPS patients were obtained from the Centre de Référence des Maladies AutoInflammatoires et des Amyloses Inflammatoires at Tenon Hospital, Paris, France. Control skin biopsies were obtained from Genoskin SAS (https://www.genoskin.com/). Genoskin has obtained all legal authorizations necessary from the French Ministry of Higher Education, Research and Innovation (AC-2017-2897) and the Personal Protection Committee (2017-A01041-52). Blood samples from three additional CAPS patients and healthy donors were obtained with prior written consent under protocols approved by the University of California, San Diego, Human Research Protections Program, and they were used to purify neutrophils or derive MCs from $CD34^+$ progenitors, as detailed below. Clinical characteristics of all CAPS patients enrolled in the study are described in Table 1.

Histological analysis and immunofluorescence

For histological analysis of MCs and leukocytes in $Kit^{W\text{-}sh/W\text{-}sh}$ $Nlrp3^{A350V}$ *Lys-Cre* mice and $Kit^{W\text{-}sh/+}$ $Nlrp3^{A350V}$ *Lys-Cre* mice, skin tissue was fixed in 10% (vol/vol) buffered formalin and embedded in paraffin and then cut into 4-µm-thick sections. Skin sections were stained with 0.1% (vol/vol) toluidine blue, pH 1, for detection of MCs or with H&E for detection of leukocytes. For immunofluorescence staining of MCs, macrophages, DCs, or neutrophils and IL-1β, IL-18, or caspase-1 in $Nlrp3^{A350V}$ *Lys-Cre* or $Nlrp3^{A350V}$ *MRP8-Cre* mice, skin tissue was fixed with 1% paraformaldehyde, dehydrated with increasing sucrose concentrations (10%, 20%, and 30%), and embedded in optimal cutting temperature compound (Tissue-Tek). Sections measuring 8 µm in thickness were cut using a cryostat. Human skin biopsies were fixed and embedded in paraffin, and 4-µm-thick sections were cut using a microtome. Frozen mouse skin sections or paraffin-embedded human skin biopsies pretreated using a heat-induced epitope retrieval method (in 10 mM sodium citrate buffer, pH 6.0) were permeabilized for 30 min in PBS supplemented with 0.5% BSA and 0.1% saponin. Permeabilized skin sections were incubated overnight at 4°C with primary antibodies: mouse Ly6G/Ly6C antibody (RB6-8C5, catalog no. 14-5931-82, 1:50; eBioscience), mouse F4/80 antibody (BM8, catalog no. 14-4801-81, 1:50; eBioscience), mouse CD11c antibody (N418, catalog no. 53-0114-82, 1:50; eBioscience), sulforhodamine-coupled avidin (catalog no. S7635-50MG, 1:1,000; Sigma-Aldrich), mouse IL-1β/IL-1F2 antibody (polyclonal, catalog no. AF-401-NA, 1:50; Bio-Techne), mouse IL-18 antibody (YIGIF74-1G7, catalog no. BE0237, 1:50; Bio X Cell), mouse caspase-1 antibody (polyclonal, catalog no. PA5-38099, 1:50; Thermo Fisher Scientific), human MPO antibody (polyclonal, catalog no. AF3667, 1:50; Bio-Techne), and human IL-1β antibody (GT289, catalog no. GTX634188, 1:50; Euromedex). They were then extensively washed and incubated with appropriate secondary antibodies for 2 h at room temperature in the dark. Skin sections were later washed in PBS and mounted between slide and coverslip. 512 × 512–pixel images were acquired using a Zeiss LSM710 Meta inverted confocal laser-scanning microscope and were processed using ImageJ software. For quantification of cell numbers and identification of caspase-1–, IL-1β–, or IL-18–positive cells in sections of mouse skin, images of three to five consecutive microscopic fields from each mouse were obtained with a 20× objective. For each image, neutrophils, MCs, macrophages, or DCs were counted, and numbers of caspase-1–, IL-1β–, or IL-18–secreting cells were determined. Statistical analyses were performed using GraphPad Prism software (GraphPad Software).

Peripheral blood mononuclear cell–derived human MCs (PBCMCs)

Human subject protocols were approved by the institutional review boards of the National Institute of Arthritis and Musculoskeletal and Skin Diseases and Stanford University. $CD34^+$ precursor cells were isolated from peripheral blood mononuclear cells of CAPS patients and healthy donors who gave written consent (EasySep Human CD34 Positive Selection Kit; STEMCELL Technologies). $CD34^+$ cells were maintained for 1 wk under serum-free conditions using StemSpan medium (STEMCELL Technologies) supplemented with recombinant human IL-6 (50 ng/ml; PeproTech), human IL-3 (10 ng/ml; PeproTech), and 3% supernatant of Chinese hamster ovary transfectants

secreting murine stem cell factor (SCF; 3% [corresponding to ∼50 ng/ml SCF]; a gift from Dr. P. Dubreuil, Marseille, France). Thereafter, the cells were maintained in IMDM GlutaMAX I, sodium pyruvate, 2-ME, 0.5% BSA, insulin-transferrin selenium (all from Invitrogen), ciprofloxacin (10 µg/ml; Sigma-Aldrich), IL-6 (50 ng/ml), and 3% supernatant of Chinese hamster ovary transfectants secreting mouse SCF. Before their use in experiments, PBCMCs were tested for phenotype by flow cytometry (anti-CD117 antibody [E-3, catalog no. sc-365504, 1:100; Santa Cruz Biotechnology], anti–Fcε receptor I antibody [AER-37, catalog no. 334639, 1:100; BioLegend]). PBCMCs were ready for experiments after ∼10 wk in culture. (MCs [positive for CD117 and Fcε receptor I] represented >95% of all cells.) In Fig. S1 D, PBCMCs were incubated in culture medium with or without pure LPS (100 ng/ml; Alexis Biochemicals) for 16 h, and levels of IL-1β in the culture supernatants were measured by ELISA (Invitrogen).

Single-cell analysis of PBCMC degranulation dynamics

The degranulation dynamics of single PBCMCs was analyzed as previously described (Gaudenzio et al., 2016). 5×10^4 human IgE-sensitized or nonsensitized PBCMCs were placed into poly-D-lysine–coated (5 µg/ml in water, catalog no. P6407; Sigma Aldrich) Nunc Lab-Tek 1.0 borosilicate cover glass system, eight chambers (catalog no. 155411; Thermo Fisher Scientific) in Tyrode's buffer supplemented with 5 µg/ml avidin-sulforhodamine 101 (catalog no. A2348; Sigma-Aldrich), as previously described (Gaudenzio et al., 2016). Stimuli were added, and then fluorescence was recorded every 2.3 s in a controlled atmosphere (using a Zeiss stagetop incubation system with objective heater, 37°C, and 5% humidified CO_2) using a Zeiss LSM710 or a Zeiss LSM780 Meta inverted confocal laser-scanning microscope, 20×/0.8 NA (working distance = 0.55) M27 objective, and electronic zoom 1 (8 bits/pixel, 512 × 512 pixels) for single-cell avidin-sulforhodamine fluorescence monitoring, and 63×/1.40 NA oil differential interference contrast M27 objective and electronic zoom 3 (dimensions: x = 512; y = 512; scaling: x = 0.264 µm; y = 0.264 µm) for high-resolution single-cell analyses. Mean fluorescence intensity was quantified using the measurement function of ImageJ software on randomly selected fields and untreated image sequences.

β-Hexosaminidase release assay

PBCMCs were incubated in culture medium with or without human IgE (1 µg ml^{-1}; Sigma-Aldrich) overnight at 37°C. The cells were then washed and distributed in 96-well, flat-bottom plates at a density of 10^5 cells in 50 µl of Tyrode's buffer at 37°C. 40 min later, cells were treated with 50 µl of prewarmed stimuli diluted in Tyrode's buffer for 45 min at 37°C. PBCMCs were then stimulated with different concentrations of anti-IgE. β-Hexosaminidase release into the supernatants was measured as previously described (Gaudenzio et al., 2016).

Peripheral blood human neutrophils

Human subject protocols were approved by the institutional review boards of the National Institute of Arthritis and Musculoskeletal and Skin Diseases and Stanford University. Peripheral blood neutrophils of CAPS patients and healthy donors who gave written consent were purified by negative selection using a commercially available kit (EasySep Human Neutrophil Isolation Kit; STEMCELL Technologies). Neutrophils were incubated with or without pure LPS (100 ng/ml; Alexis Biochemicals) for 16 h, and levels of IL-1β and IL-18 in the culture supernatants were measured by ELISA (Invitrogen).

IgE-mediated PSA

IgE-dependent PSA was induced as described previously (Lilla et al., 2011). Briefly, mice were sensitized passively with IgE by i.p. injection of 20 µg of DNP-specific IgE (clone ε26 [Liu et al., 1980], kindly provided by Dr. Fu-Tong Liu, Department of Dermatology, University of California, Davis, Davis, CA) in 100 µl of PBS and then challenged i.p. the next day with 1 mg DNP–human serum albumin (A6661; Sigma-Aldrich) in 100 µl of PBS. Immediately before and at intervals after antigen challenge, body temperature was measured with a rectal thermometer (Physitemp Instruments).

Treatment with anti–IL-1β and anti–IL-18 neutralizing antibodies

Nlrp3^{A350V} *MRP8-Cre* pups were treated s.c. with Armenian hamster IgG anti-mouse IL-1β (clone B122, catalog no. BE0246, 10 µg/g; Bio X Cell) mixed with rat IgG2aκ isotype controls (clone 2A3, catalog no. BE0089, 10 µg/g; Bio X Cell) in PBS (20 µl/g) or rat IgG2aκ antimouse IL-18 (clone YIGIF74-1G7, catalog no. BE0237, 10 µg/g; Bio X Cell) mixed with an Armenian hamster IgG isotype control (catalog no. BE0091, 10 µg/g; Bio X Cell) in PBS (20 µl/g) every other day beginning on day 2 of life for a total of six doses, as outlined in Fig. S3 C.

Statistical analysis

Data were analyzed for statistical significance using the Mantel-Haenszel log-rank test, unpaired Mann-Whitney *U* test, or two-way ANOVA, as indicated in the figure legends. $P < 0.05$ was considered statistically significant.

Online supplemental material

Fig. S1 shows numbers of MCs and IL-1β expression in MCs from *Nlrp3*^{A350V} *Lys-Cre* mice, responses of *Nlrp3*^{L351P} *Mcpt5-Cre* mice in a model of IgE-mediated anaphylaxis, and degranulation upon stimulation with IgE/anti-IgE and IL-1β production upon stimulation with LPS in MCs derived from peripheral blood of healthy donors and CAPS patients. Fig. S2 shows the gene expression analysis of *Nlrp3* and *Il1b* among major immune cell populations in humans and mice, caspase-1 and IL-18 expression in neutrophils from *Nlrp3*^{A350V} *Lys-Cre* mice, IL-1β and IL-18 release from neutrophils purified from the blood of CAPS patients, and the staining of IL-1β and neutrophil MPO in the skin of two CAPS patients. Fig. S3 shows caspase-1 expression in neutrophils from *Nlrp3*^{A350V} *MRP8-Cre* mice and body weight and survival of *Nlrp3*^{A350V} *MRP8-Cre* mice treated with anti–IL-1β or anti–IL-18 antibodies.

Acknowledgments

We thank Irving Weissman (Stanford University, Stanford, CA) and Clifford Lowell (University of California, San Francisco, San Francisco, CA) for sharing *MRP8-Cre* mice. We also thank the CAPS patients for their participation and Dr. Kieron Leslie for referral of patients.

N. Gaudenzio is supported by the European Research Council (ERC-2018-STG grant 802041) and the Institut national de la santé et de la recherche médicale ATIP-Avenir program. T. Marichal is supported by an Incentive Grant for Scientific Research of the Fund for Scientific Research of the Fonds De La Recherche Scientifique – FNRS (F.4508.18), by the Fund for Strategic Fundamental Research–Walloon Excellence in Lifesciences and Biotechnology (grant CR-2017s-04), by the Acteria Foundation, and by the European Research Council (ERC-StG-2018 grant 801823). F. Jönsson is supported by an Agence Nationale de la Recherche Young Female Researchers and Young Researchers grant (ANR-16-CE15-0012) and is an employee of the Centre National de la Recherche Scientifique. P. Bruhns was supported by the European Research Council Seventh Framework Programme (ERC-2013-CoG 616050), by the Institut Pasteur, and by the Institut national de la santé et de la recherche médicale. B. Balbino was supported partly by a stipend from the Pasteur-Paris University international doctoral program and a fellowship from the Fondation pour la Recherche Médicale. L.L. Reber was supported by the Arthritis National Research Foundation, the National Institutes of Health (grant K99 AI110645), and an ATIP-Avenir grant from the Institut national de la santé et de la recherche médicale. S.J. Galli is supported by the National Institutes of Health (grants R01 AI132494, R01 AR067145, R01 AI125567, and U19 AI104209). L. Broderick is supported by grants from the American Academy of Allergy Asthma and Immunology Foundation and the National Institutes of Health (R01 DK113592). H.M. Hoffman is supported by National Institutes of Health grants R01 AI15586901 and R01 DK113592.

Author contributions: J. Stackowicz, N. Gaudenzio, S.J. Galli, L. Broderick, H.M. Hoffman, and L.L. Reber designed the experiments. J. Stackowicz, N. Gaudenzio, N. Serhan, E. Conde, O. Godon, T. Marichal, P. Starkl, B. Balbino, and L. Broderick conducted experiments and acquired data. J. Stackowicz, P. Bruhns, F. Jönsson, N. Gaudenzio, S.J. Galli, L. Broderick, H.M. Hoffman, and L.L. Reber analyzed the data. A. Roers provided mice. H.M. Hoffman, P. Moguelet, and S. Georgin-Lavialle provided clinical samples. J. Stackowicz, N. Gaudenzio, S.J. Galli, L. Broderick, H.M. Hoffman, and L.L. Reber wrote the original draft of the manuscript. All authors contributed to review and editing of the manuscript.

Disclosures: L. Broderick reports "other" from Novartis, Inc. outside the submitted work. H.M. Hoffman reports "other" from Novartis, IFM, AB2Bio, Takeda, and Zomagen; and grants from Jecure outside the submitted work. No other disclosures were reported.

Submitted: 10 July 2020
Revised: 10 June 2021
Accepted: 30 July 2021

References

Abram, C.L., G.L. Roberge, Y. Hu, and C.A. Lowell. 2014. Comparative analysis of the efficiency and specificity of myeloid-Cre deleting strains using ROSA-EYFP reporter mice. *J. Immunol. Methods.* 408:89–100. https://doi.org/10.1016/j.jim.2014.05.009

Agostini, L., F. Martinon, K. Burns, M.F. McDermott, P.N. Hawkins, and J. Tschopp. 2004. NALP3 forms an IL-1β-processing inflammasome with increased activity in Muckle-Wells autoinflammatory disorder. *Immunity.* 20:319–325. https://doi.org/10.1016/S1074-7613(04)00046-9

Aksentijevich, I., M. Nowak, M. Mallah, J.J. Chae, W.T. Watford, S.R. Hofmann, L. Stein, R. Russo, D. Goldsmith, P. Dent, et al. 2002. De novo CIAS1 mutations, cytokine activation, and evidence for genetic heterogeneity in patients with neonatal-onset multisystem inflammatory disease (NOMID): a new member of the expanding family of pyrin-associated autoinflammatory diseases. *Arthritis Rheum.* 46:3340–3348. https://doi.org/10.1002/art.10688

Aksentijevich, I., C.D. Putnam, E.F. Remmers, J.L. Mueller, J. Le, R.D. Kolodner, Z. Moak, M. Chuang, F. Austin, R. Goldbach-Mansky, et al. 2007. The clinical continuum of cryopyrinopathies: novel CIAS1 mutations in North American patients and a new cryopyrin model. *Arthritis Rheum.* 56:1273–1285. https://doi.org/10.1002/art.22491

Brydges, S.D., J.L. Mueller, M.D. McGeough, C.A. Pena, A. Misaghi, C. Gandhi, C.D. Putnam, D.L. Boyle, G.S. Firestein, A.A. Horner, et al. 2009. Inflammasome-mediated disease animal models reveal roles for innate but not adaptive immunity. *Immunity.* 30:875–887. https://doi.org/10.1016/j.immuni.2009.05.005

Brydges, S.D., L. Broderick, M.D. McGeough, C.A. Pena, J.L. Mueller, and H.M. Hoffman. 2013. Divergence of IL-1, IL-18, and cell death in NLRP3 inflammasomopathies. *J. Clin. Invest.* 123:4695–4705. https://doi.org/10.1172/JCI71543

Camilli, G., M. Bohm, A.C. Piffer, R. Lavenir, D.L. Williams, B. Neven, G. Grateau, S. Georgin-Lavialle, and J. Quintin. 2020. β-Glucan-induced reprogramming of human macrophages inhibits NLRP3 inflammasome activation in cryopyrinopathies. *J. Clin. Invest.* 130:4561–4573. https://doi.org/10.1172/JCI134778

Chen, K.W., M. Monteleone, D. Boucher, G. Sollberger, D. Ramnath, N.D. Condon, J.B. von Pein, P. Broz, M.J. Sweet, and K. Schroder. 2018. Noncanonical inflammasome signaling elicits gasdermin D-dependent neutrophil extracellular traps. *Sci. Immunol.* 3:eaar6676. https://doi.org/10.1126/sciimmunol.aar6676

Dowds, T.A., J. Masumoto, L. Zhu, N. Inohara, and G. Núñez. 2004. Cryopyrin-induced interleukin 1beta secretion in monocytic cells: enhanced activity of disease-associated mutants and requirement for ASC. *J. Biol. Chem.* 279:21924–21928. https://doi.org/10.1074/jbc.M401178200

Dudeck, A., J. Dudeck, J. Scholten, A. Petzold, S. Surianarayanan, A. Köhler, K. Peschke, D. Vöhringer, C. Waskow, T. Krieg, et al. 2011. Mast cells are key promoters of contact allergy that mediate the adjuvant effects of haptens. *Immunity.* 34:973–984. https://doi.org/10.1016/j.immuni.2011.03.028

Fenini, G., E. Contassot, and L.E. French. 2017. Potential of IL-1, IL-18 and inflammasome inhibition for the treatment of inflammatory skin diseases. *Front. Pharmacol.* 8:278. https://doi.org/10.3389/fphar.2017.00278

Finkelman, F.D. 2007. Anaphylaxis: lessons from mouse models. *J. Allergy Clin. Immunol.* 120:506–515, quiz: 516–517. https://doi.org/10.1016/j.jaci.2007.07.033

Gaudenzio, N., R. Sibilano, T. Marichal, P. Starkl, L.L. Reber, N. Cenac, B.D. McNeil, X. Dong, J.D. Hernandez, R. Sagi-Eisenberg, et al. 2016. Different activation signals induce distinct mast cell degranulation strategies. *J. Clin. Invest.* 126:3981–3998. https://doi.org/10.1172/JCI85538

Heng, T.S., M.W. Painter, K. Elpek, V. Lukacs-Kornek, N. Mauermann, S.J. Turley, D. Koller, F.S. Kim, A.J. Wagers, N. Asinovski, et al. Immunological Genome Project Consortium. 2008. The Immunological Genome Project: networks of gene expression in immune cells. *Nat. Immunol.* 9:1091–1094. https://doi.org/10.1038/ni1008-1091

Hoffman, H.M., and L. Broderick. 2016. The role of the inflammasome in patients with autoinflammatory diseases. *J. Allergy Clin. Immunol.* 138:3–14. https://doi.org/10.1016/j.jaci.2016.05.001

Hoffman, H.M., J.L. Mueller, D.H. Broide, A.A. Wanderer, and R.D. Kolodner. 2001a. Mutation of a new gene encoding a putative pyrin-like protein causes familial cold autoinflammatory syndrome and Muckle-Wells syndrome. *Nat. Genet.* 29:301–305. https://doi.org/10.1038/ng756

Hoffman, H.M., A.A. Wanderer, and D.H. Broide. 2001b. Familial cold autoinflammatory syndrome: phenotype and genotype of an autosomal dominant periodic fever. *J. Allergy Clin. Immunol.* 108:615–620. https://doi.org/10.1067/mai.2001.118790

Hoffman, H.M., S. Rosengren, D.L. Boyle, J.Y. Cho, J. Nayar, J.L. Mueller, J.P. Anderson, A.A. Wanderer, and G.S. Firestein. 2004. Prevention of cold-associated acute inflammation in familial cold autoinflammatory syndrome by interleukin-1 receptor antagonist. *Lancet.* 364:1779–1785. https://doi.org/10.1016/S0140-6736(04)17401-1

Hoffman, H.M., M.L. Throne, N.J. Amar, M. Sebai, A.J. Kivitz, A. Kavanaugh, S.P. Weinstein, P. Belomestnov, G.D. Yancopoulos, N. Stahl, et al. 2008.

Efficacy and safety of rilonacept (interleukin-1 Trap) in patients with cryopyrin-associated periodic syndromes: results from two sequential placebo-controlled studies. *Arthritis Rheum.* 58:2443–2452. https://doi.org/10.1002/art.23687

Hoffman, H.M., M.L. Throne, N.J. Amar, R.C. Cartwright, A.J. Kivitz, Y. Soo, and S.P. Weinstein. 2012. Long-term efficacy and safety profile of rilonacept in the treatment of cryopryin-associated periodic syndromes: results of a 72-week open-label extension study. *Clin. Ther.* 34: 2091–2103. https://doi.org/10.1016/j.clinthera.2012.09.009

Jo, E.K., J.K. Kim, D.M. Shin, and C. Sasakawa. 2016. Molecular mechanisms regulating NLRP3 inflammasome activation. *Cell. Mol. Immunol.* 13: 148–159. https://doi.org/10.1038/cmi.2015.95

Johnson, J.L., M. Ramadass, A. Haimovich, M.D. McGeough, J. Zhang, H.M. Hoffman, and S.D. Catz. 2017. Increased neutrophil secretion induced by *NLRP3* mutation links the inflammasome to azurophilic granule exocytosis. *Front. Cell. Infect. Microbiol.* 7:507. https://doi.org/10.3389/fcimb.2017.00507

Kool, M., V. Pétrilli, T. De Smedt, A. Rolaz, H. Hammad, M. van Nimwegen, I.M. Bergen, R. Castillo, B.N. Lambrecht, and J. Tschopp. 2008. Cutting edge: alum adjuvant stimulates inflammatory dendritic cells through activation of the NALP3 inflammasome. *J. Immunol.* 181:3755–3759. https://doi.org/10.4049/jimmunol.181.6.3755

Lachmann, H.J., I. Kone-Paut, J.B. Kuemmerle-Deschner, K.S. Leslie, E. Hachulla, P. Quartier, X. Gitton, A. Widmer, N. Patel, and P.N. Hawkins. Canakinumab in CAPS Study Group. 2009. Use of canakinumab in the cryopyrin-associated periodic syndrome. *N. Engl. J. Med.* 360:2416–2425. https://doi.org/10.1056/NEJMoa0810787

Latz, E., T.S. Xiao, and A. Stutz. 2013. Activation and regulation of the inflammasomes. *Nat. Rev. Immunol.* 13:397–411. https://doi.org/10.1038/nri3452

Ley, K., H.M. Hoffman, P. Kubes, M.A. Cassatella, A. Zychlinsky, C.C. Hedrick, and S.D. Catz. 2018. Neutrophils: new insights and open questions. *Sci. Immunol.* 3:eaat4579. https://doi.org/10.1126/sciimmunol.aat4579

Lilla, J.N., C.C. Chen, K. Mukai, M.J. BenBarak, C.B. Franco, J. Kalesnikoff, M. Yu, M. Tsai, A.M. Piliponsky, and S.J. Galli. 2011. Reduced mast cell and basophil numbers and function in *Cpa3-Cre; Mcl-1*$^{fl/fl}$ mice. *Blood.* 118: 6930–6938. https://doi.org/10.1182/blood-2011-03-343962

Liu, F.T., J.W. Bohn, E.L. Ferry, H. Yamamoto, C.A. Molinaro, L.A. Sherman, N.R. Klinman, and D.H. Katz. 1980. Monoclonal dinitrophenyl-specific murine IgE antibody: preparation, isolation, and characterization. *J. Immunol.* 124:2728–2737.

Louvrier, C., E. Assrawi, E. El Khouri, I. Melki, B. Copin, E. Bourrat, N. Lachaume, B. Cador-Rousseau, P. Duquesnoy, W. Piterboth, et al. 2020. NLRP3-associated autoinflammatory diseases: phenotypic and molecular characteristics of germline versus somatic mutations. *J. Allergy Clin. Immunol.* 145:1254–1261. https://doi.org/10.1016/j.jaci.2019.11.035

Martinon, F., K. Burns, and J. Tschopp. 2002. The inflammasome: a molecular platform triggering activation of inflammatory caspases and processing of proIL-β. *Mol. Cell.* 10:417–426. https://doi.org/10.1016/S1097-2765(02)00599-3

Martinon, F., V. Pétrilli, A. Mayor, A. Tardivel, and J. Tschopp. 2006. Gout-associated uric acid crystals activate the NALP3 inflammasome. *Nature.* 440:237–241. https://doi.org/10.1038/nature04516

McGeough, M.D., A. Wree, M.E. Inzaugarat, A. Haimovich, C.D. Johnson, C.A. Peña, R. Goldbach-Mansky, L. Broderick, A.E. Feldstein, and H.M. Hoffman. 2017. TNF regulates transcription of NLRP3 inflammasome components and inflammatory molecules in cryopyrinopathies. *J. Clin. Invest.* 127:4488–4497. https://doi.org/10.1172/JCI90699

Meng, G., F. Zhang, I. Fuss, A. Kitani, and W. Strober. 2009. A mutation in the Nlrp3 gene causing inflammasome hyperactivation potentiates Th17 cell-dominant immune responses. *Immunity.* 30:860–874. https://doi.org/10.1016/j.immuni.2009.04.012

Nakamura, Y., N. Kambe, M. Saito, R. Nishikomori, Y.G. Kim, M. Murakami, G. Núñez, and H. Matsue. 2009. Mast cells mediate neutrophil recruitment and vascular leakage through the NLRP3 inflammasome in histamine-independent urticaria. *J. Exp. Med.* 206:1037–1046. https://doi.org/10.1084/jem.20082179

Nakamura, Y., L. Franchi, N. Kambe, G. Meng, W. Strober, and G. Núñez. 2012. Critical role for mast cells in interleukin-1β-driven skin inflammation associated with an activating mutation in the Nlrp3 protein. *Immunity.* 37:85–95. https://doi.org/10.1016/j.immuni.2012.04.013

Németh, T., M. Sperandio, and A. Mócsai. 2020. Neutrophils as emerging therapeutic targets. *Nat. Rev. Drug Discov.* 19:253–275. https://doi.org/10.1038/s41573-019-0054-z

Neven, B., I. Callebaut, A.M. Prieur, J. Feldmann, C. Bodemer, L. Lepore, B. Derfalvi, S. Benjaponpitak, R. Vesely, M.J. Sauvain, et al. 2004. Molecular basis of the spectral expression of CIAS1 mutations associated with phagocytic cell-mediated autoinflammatory disorders CINCA/NOMID, MWS, and FCU. *Blood.* 103:2809–2815. https://doi.org/10.1182/blood-2003-07-2531

Passegué, E., E.F. Wagner, and I.L. Weissman. 2004. JunB deficiency leads to a myeloproliferative disorder arising from hematopoietic stem cells. *Cell.* 119:431–443. https://doi.org/10.1016/j.cell.2004.10.010

Reber, L.L., T. Marichal, and S.J. Galli. 2012. New models for analyzing mast cell functions in vivo. *Trends Immunol.* 33:613–625. https://doi.org/10.1016/j.it.2012.09.008

Reber, L.L., C.M. Gillis, P. Starkl, F. Jönsson, R. Sibilano, T. Marichal, N. Gaudenzio, M. Bérard, S. Rogalla, C.H. Contag, et al. 2017a. Neutrophil myeloperoxidase diminishes the toxic effects and mortality induced by lipopolysaccharide. *J. Exp. Med.* 214:1249–1258. https://doi.org/10.1084/jem.20161238

Reber, L.L., J.D. Hernandez, and S.J. Galli. 2017b. The pathophysiology of anaphylaxis. *J. Allergy Clin. Immunol.* 140:335–348. https://doi.org/10.1016/j.jaci.2017.06.003

Sharp, F.A., D. Ruane, B. Claass, E. Creagh, J. Harris, P. Malyala, M. Singh, D.T. O'Hagan, V. Pétrilli, J. Tschopp, et al. 2009. Uptake of particulate vaccine adjuvants by dendritic cells activates the NALP3 inflammasome. *Proc. Natl. Acad. Sci. USA.* 106:870–875. https://doi.org/10.1073/pnas.0804897106

Shay, T., V. Jojic, O. Zuk, K. Rothamel, D. Puyraimond-Zemmour, T. Feng, E. Wakamatsu, C. Benoist, D. Koller, and A. Regev. ImmGen Consortium. 2013. Conservation and divergence in the transcriptional programs of the human and mouse immune systems. *Proc. Natl. Acad. Sci. USA.* 110: 2946–2951. https://doi.org/10.1073/pnas.1222738110

Sollberger, G., A. Choidas, G.L. Burn, P. Habenberger, R. Di Lucrezia, S. Kordes, S. Menninger, J. Eickhoff, P. Nussbaumer, B. Klebl, et al. 2018. Gasdermin D plays a vital role in the generation of neutrophil extracellular traps. *Sci. Immunol.* 3:eaar6689. https://doi.org/10.1126/sciimmunol.aar6689

Tschopp, J., and K. Schroder. 2010. NLRP3 inflammasome activation: the convergence of multiple signalling pathways on ROS production? *Nat. Rev. Immunol.* 10:210–215. https://doi.org/10.1038/nri2725

Supplemental material

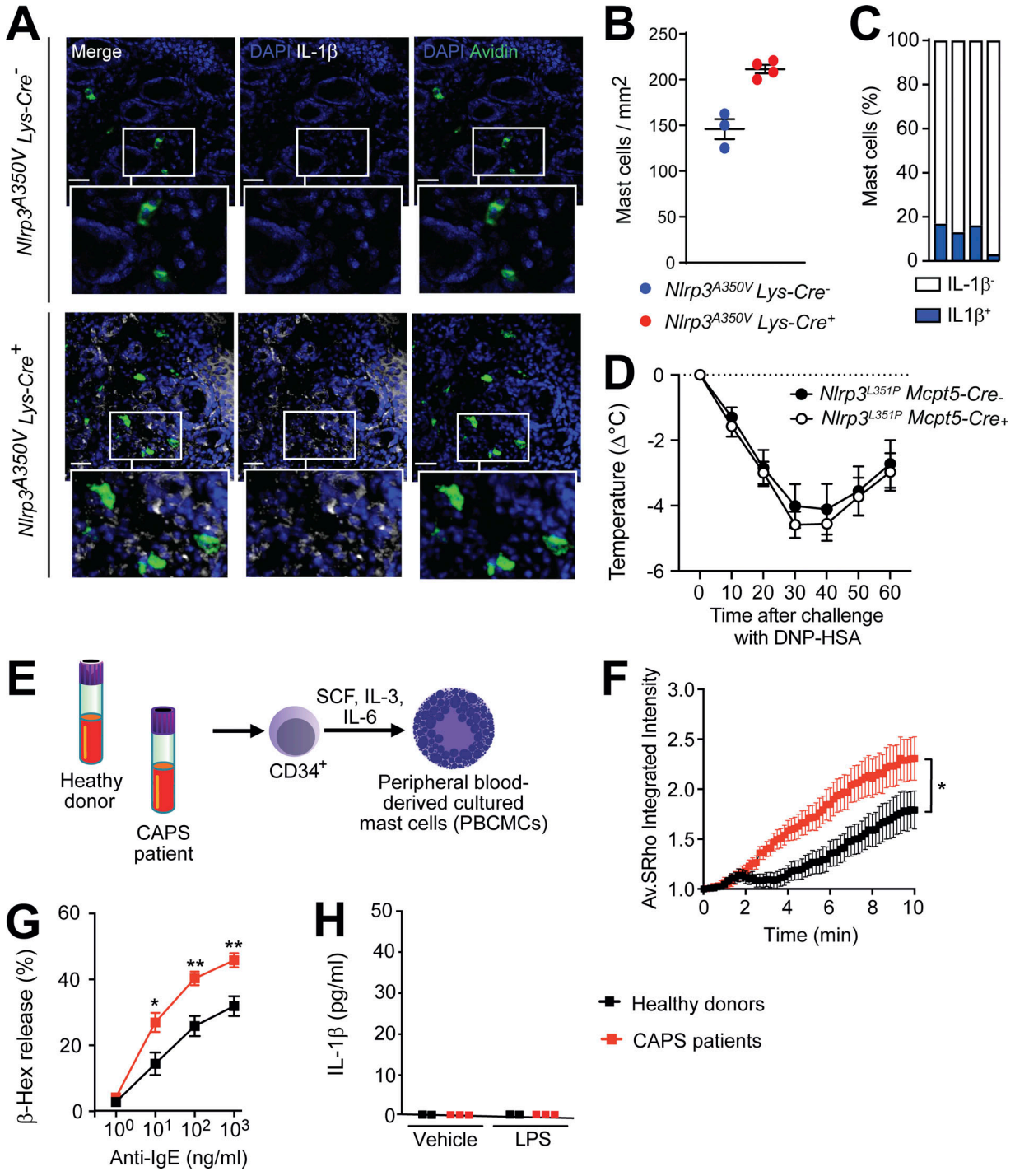

Figure S1. **Phenotype of MCs in *Nlrp3* mutant mice and CAPS patients. (A)** Representative confocal microscopy showing staining of skin tissue sections from *Nlrp3*^{A350V} *Lys-Cre*$^{+}$ mice and *Nlrp3*^{A350V} *Lys-Cre*$^{-}$ controls stained with DAPI (which stains nuclei), anti–IL-1β antibodies, and sulforhodamine (SRho)-coupled avidin (which stains MCs). Scale bars: 50 µm. **(B)** Quantification of avidin^{+} MCs in skin sections. Results show values from individual mice, with bars indicating mean ± SEM. **(C)** Percentage of IL-1β^{+} and IL-1β^{-} MCs (avidin^{+}) in skin sections. **(D)** Responses of *Nlrp3*^{L351P} *Mcpt5-Cre*$^{-}$ (n = 8) and responses of *Nlrp3*^{L351P} *Mcpt5-Cre*$^{+}$ (n = 7) mice in a model of IgE-mediated passive systemic anaphylaxis (PSA). Mice were sensitized i.p. with anti-DNP IgE and challenged i.p. 24 h later with DNP–human serum albumin (HSA). Data are pooled from two independent experiments and show changes in body temperature (Δ°C [mean ± SEM]) after challenge. **(E)** CD34^{+} progenitors were purified by positive selection from the blood of healthy donors and CAPS patients and differentiated in vitro for 12 wk into PBCMCs. **(F)** IgE-sensitized PBCMCs were stimulated with 2 µg/ml anti-IgE in the presence of SRho-coupled avidin (Av.SRho). Data show mean time-lapse sequence ± SEM of SRho-avidin quantification (mean fluorescence intensity) from pooled single-cell analyses (n = 16–19) from PBCMCs from three healthy donors and three CAPS patients. *, P < 0.05 (two-way ANOVA). **(G)** IgE-sensitized PBCMCs were stimulated with anti-IgE at the indicated concentration. MC degranulation was quantified using β-hexosaminidase release (β-Hex) assay. Data are presented as mean ± SEM and are pooled from PBCMCs from three healthy donors and three CAPS patients. *, P < 0.05; **, P < 0.01 (Mann-Whitney *U* test). **(H)** Quantification of IL-1β release at 16 h upon stimulation with LPS (100 ng/ml) or PBS ("vehicle" as a control) in PBCMCs from healthy donors or CAPS patients. Results show values from individual donors.

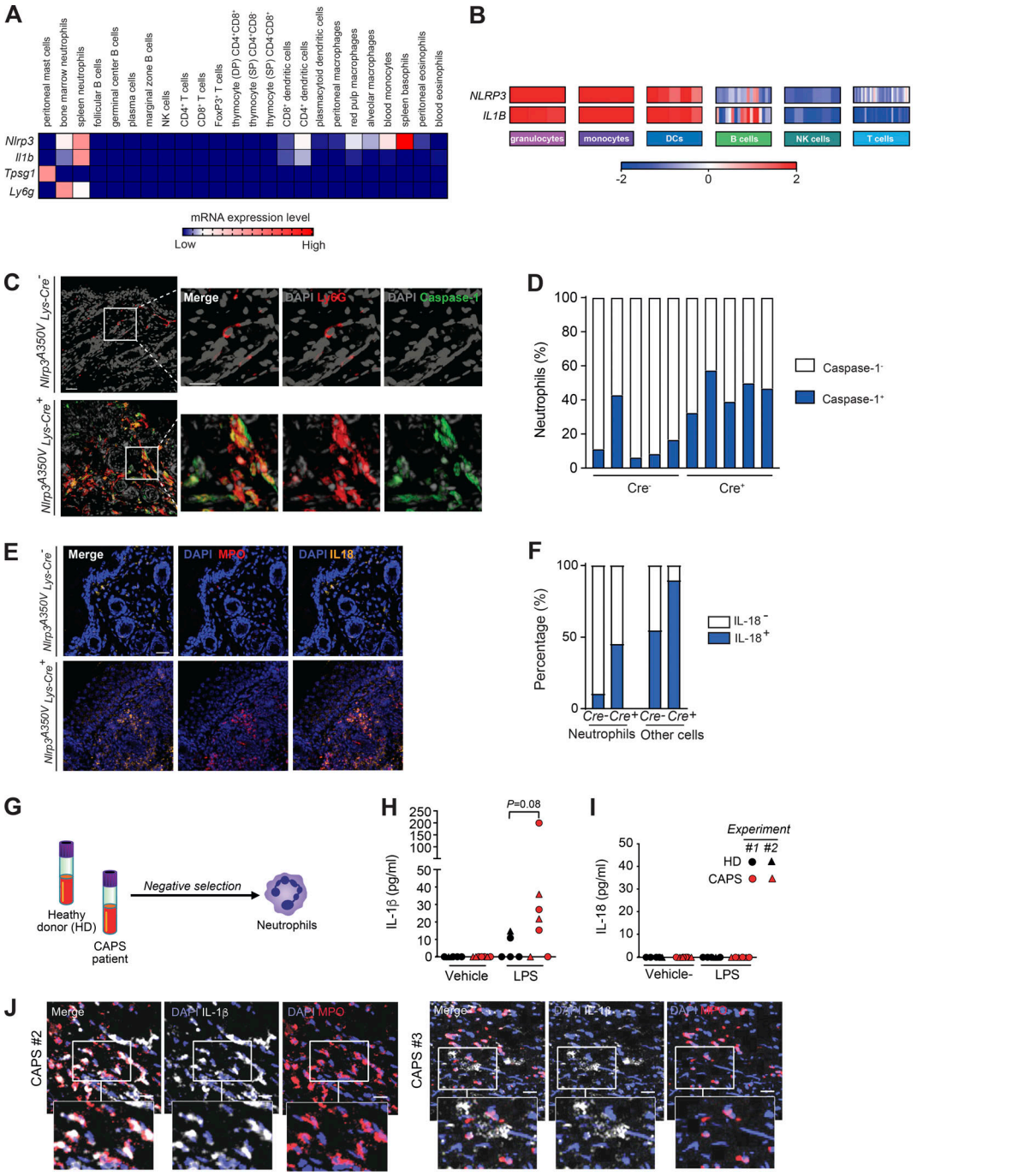

Figure S2. **Gene expression analysis of mouse and human NLRP3 and IL1B, expression of caspase-1 and IL-18 in neutrophils from *Nlrp3*^{A350V} *Lys-Cre* mice, and production of IL-1β and IL-18 in neutrophils from CAPS patients. (A)** Publicly available RNA-sequencing data of *Nlrp3*, *Il1b*, *Tpsg1* (tryptase gamma, expressed in MCs), and *Ly6g* (expressed in neutrophils) in different mouse immune cell subpopulations (http://rstats.immgen.org/Skyline/skyline.html; Heng et al., 2008); data are shown using a heat map of mRNA expression levels. NK, natural killer; DP, double positive; SP, single positive. **(B)** Publicly available microarray data of NLRP3 and IL1B in different human immune cell populations (http://rstats.immgen.org/comparative/comparative_search.php; Shay et al., 2013); data are shown using a heat map of mean-centered expression values (red/blue color bar on the bottom). **(C)** Representative confocal microscopy showing staining of skin tissue sections from *Nlrp3*^{A350V} *Lys-Cre*$^{+}$ mice and *Nlrp3*^{A350V} *Lys-Cre*$^{-}$ controls stained with DAPI (which stains nuclei), anti–caspase-1 antibodies, and anti-Ly6G antibodies (which stains neutrophils). Scale bars: 30 µm. **(D)** Percentage of caspase-1^{+} and caspase-1^{-} neutrophils (Ly6G^{+}) in skin sections. **(E)** Representative confocal microscopy showing staining of skin tissue sections from *Nlrp3*^{A350V} *Lys-Cre*$^{+}$ mice and *Nlrp3*^{A350V} *Lys-Cre*$^{-}$ controls stained with DAPI, anti–IL-18 antibodies, and anti-MPO antibodies. Scale bars: 20 µm. **(F)** Percentage of IL-18^{-} and IL-18^{+} cells in the MPO^{+} neutrophil population versus other cells in skin sections. Scale bar: 30 µm. **(G–I)** Neutrophils were purified by negative selection from the blood of five control subjects and four CAPS patients (G). For three patients, neutrophils were purified at two different occasions 6 mo apart (experiments 1 and 2). Neutrophils were incubated with LPS (100 ng/ml) or vehicle (PBS) for 16 h. IL-1β (H) and IL-18 (I) concentrations in the medium were quantified by ELISA. **(J)** Skin tissue sections from two CAPS patients stained with DAPI, anti–IL-1β, and anti-MPO antibodies. Scale bars: 50 µm. Lower panels are enlargements of the boxed areas. Patient 1 is depicted in Fig. 3 E.

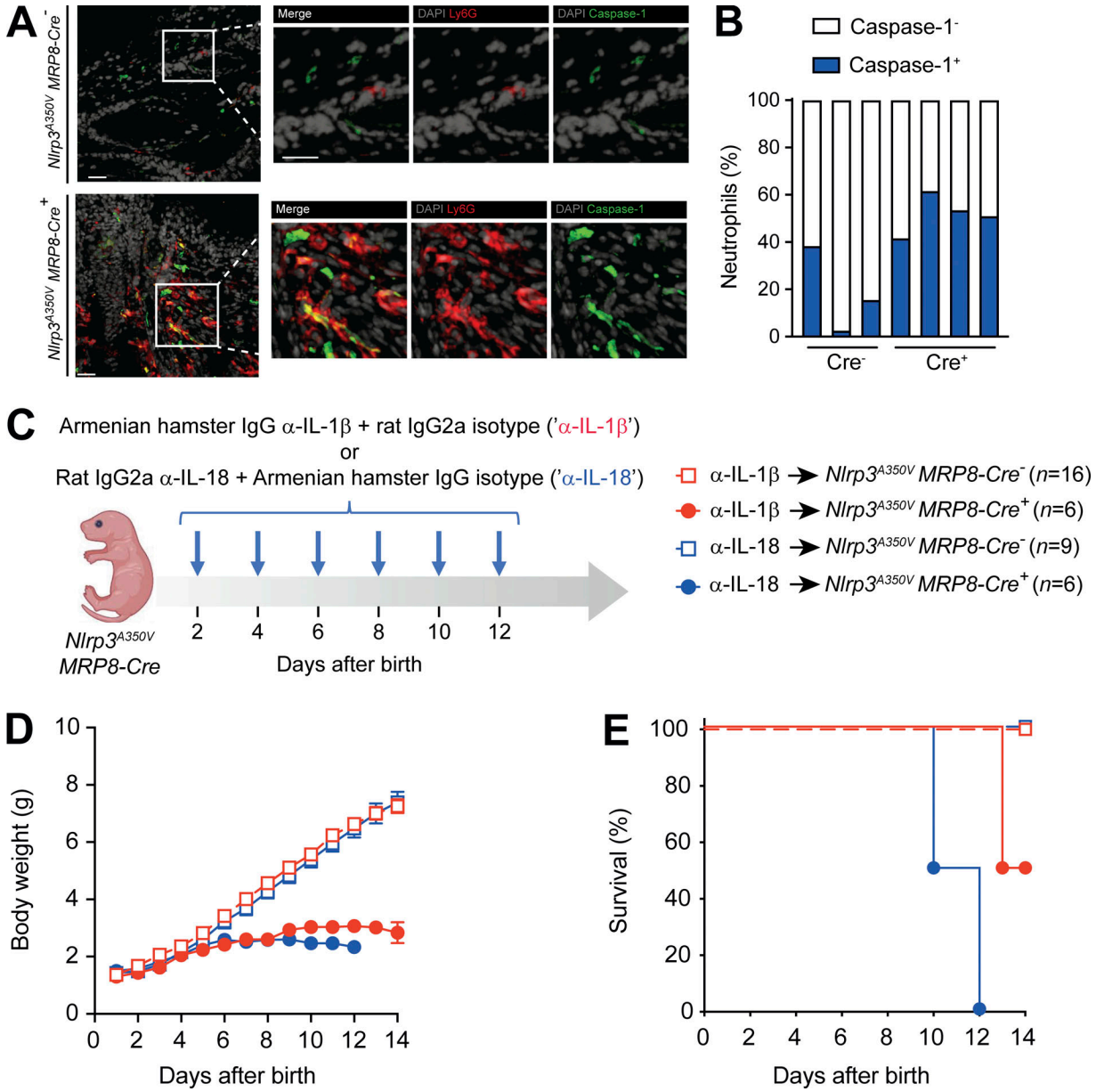

Figure S3. **Expression of caspase-1 in skin neutrophils and effect of treatment with anti–IL-1β or anti–IL-18 antibodies in *Nlrp3*^{A350V} *MRP8-Cre* mice.** **(A)** Representative confocal microscopy showing staining of skin tissue sections from *Nlrp3*^{A350V} *MRP8-Cre*$^{+}$ mice and *Nlrp3*^{A350V} *MRP8-Cre*$^{-}$ controls stained with DAPI (which stains nuclei), anti–caspase-1 antibodies, and anti-Ly6G antibodies (which stain neutrophils). Scale bars: 30 µm. **(B)** Percentage of caspase-1^{+} and caspase-1^{-} neutrophils (Ly6G^{+}) in skin sections. **(C–E)** Treatment of *Nlrp3*^{A350V} *MRP8-Cre* mice with anti–IL-1β or anti–IL-18 antibodies. Protocol outline (C), body weight (D), and survival (E) at the indicated time points. In D, data are presented as mean ± SEM.